Nickel(II/IV) Manifold Enables Room Temperature C(sp^3)–H Functionalization

Courtney C. Roberts,[†,#] Eugene Chong,[†,#] Jeff W. Kampf,[†] Allan J. Canty,[‡] Alireza Ariafard,[‡] and Melanie S. Sanford[†]*

[†]Department of Chemistry, University of Michigan, 930 N. University Avenue, Ann Arbor, Michigan 48109, United States

[‡]School of Natural Sciences - Chemistry, University of Tasmania, Hobart, Tasmania 7001, Australia

ABSTRACT: This Article demonstrates a mild oxidatively-induced C(sp^3)–H activation at a high valent Ni center. In contrast to most C(sp^3)–H activation reactions at Ni^{II}, the transformation proceeds at room temperature and generates an isolable Ni^{IV} σ-alkyl complex. DFT studies show two plausible mechanisms for this C–H activation process, involving triflate-assisted C–H cleavage at either a Ni^{IV} or a Ni^{III} intermediate. The former pathway is modestly favored over the latter (by ~3 kcal/mol). The Ni^{IV} σ-alkyl product of C–H cleavage reacts with a variety of nucleophiles to form C(sp^3)–X bonds (X = halide, oxygen, nitrogen, sulfur, carbon). These stoichiometric transformations can be coupled using *N*-fluoro-2,4,6-trimethylpyridinium triflate as a terminal oxidant in conjunction with chloride as a nucleophile to achieve a proof-of-principle $Ni^{II/IV}$-catalyzed C(sp^3)–H functionalization reaction.

Over the past decade, nickel-catalyzed C–H bond functionalization reactions have emerged as valuable methods for the formation of new carbon–carbon and carbon–heteroatom bonds.[1] Nickel-based catalysts offer the advantages of high abundance and low cost, particularly relative to the more commonly studied palladium analogues.[2] In addition, Ni catalysis can enable complementary functionalization pathways relative to Pd systems, based on the propensity of Ni to participate in both one and two electron redox processes.[2,3,4] The mechanism for known Ni-catalyzed C–H functionalization reactions is shown in Figure 1a. C–H activation (step i) is proposed to occur at a low valent Ni^{II} center (**A**) to afford a Ni^{II} σ-aryl or σ-alkyl intermediate (**B**).[1d,1f,5] Oxidative functionalization of this intermediate then releases the product and regenerates the Ni^{II} catalyst (step ii). This mechanistic manifold has proven effective for the functionalization of both C(sp^2)–H and C(sp^3)–H bonds in several contexts (most commonly, C–H bonds proximal to aminoquinoline directing groups).[6] However, the substrate scope of Ni-catalyzed C–H functionalization is currently far narrower than that of analogous transformations at Pd.[1a-d,7] Additionally, most Ni-catalyzed C–H functionalization reactions require forcing conditions (generally temperatures in excess of 130 ºC).[6] Both of these limitations stem, at least in part, from the C–H activation step, which is known to be considerably more challenging at Ni^{II} than at analogous Pd^{II} centers.[5]

We hypothesized that these limitations could potentially be addressed by changing the oxidation state at Ni during the C–H activation step (Figure 1b).[7a] Specifically, we sought to develop a transformation in which C–H activation occurs at a more electrophilic high valent Ni center rather than at a Ni^{II} intermediate (for instance, a Ni^{IV} complex like **C** in Figure 1b, step i).[7a,8] This could then be followed by functionalization of the resulting Ni^{IV} σ-aryl or σ-alkyl intermediate (**D**) (step ii)[9] and subsequent oxidation of Ni^{II} (step iii) to regenerate the catalyst. The viability of this approach is preliminarily supported by our recent report showing that stoichiometric C(sp^2)–H activation can occur at high valent Ni centers under remarkably

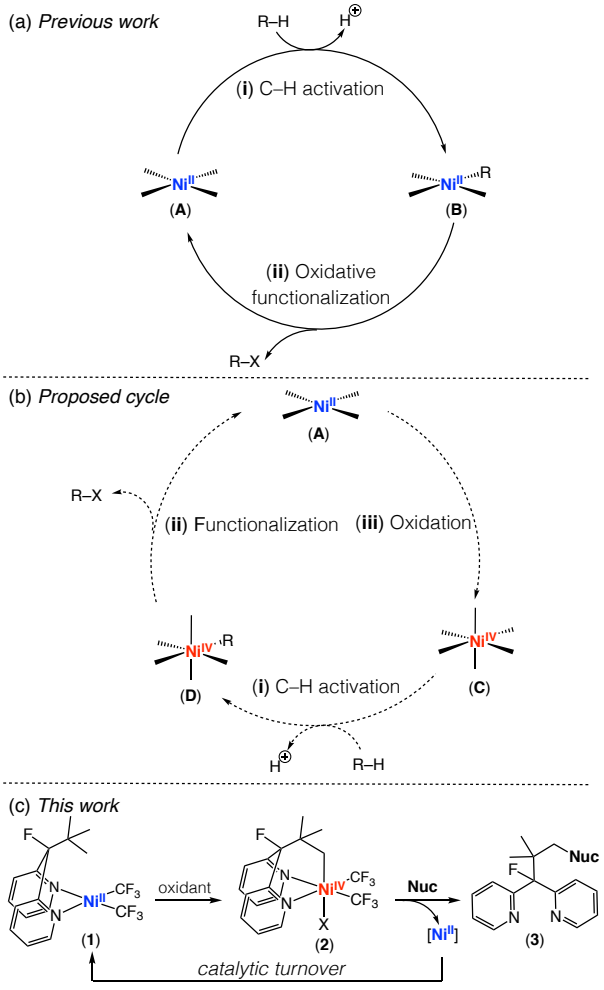

Figure 1. (a) Mechanism for known Ni-catalyzed C–H functionalization reactions (involving C–H activation at Ni^{II}). (b) New pathway involving C–H activation at Ni^{IV}. (c) This study.

mild conditions (10 min at 25 ºC).[10] However, as described in detail below, the Ni^{IV} σ-aryl product is inert towards subsequent functionalization (step ii), thus precluding catalytic turnover in this system.

In this Article, we demonstrate a C(sp^3)–H activation reaction at high valent Ni that occurs within minutes at room temperature. Further, we show that, under appropriate conditions, the Ni^{IV} σ-alkyl product undergoes functionalization with both heteroatom and carbon-based nucleophiles. Detailed investigations of both the C–H activation and functionalization steps are described. Ultimately, these studies are leveraged to achieve a proof-of-principle catalytic cycle in which this mild C–H activation at high valent Ni is coupled with nucleophilic functionalization to achieve several turnovers of a C(sp^3)–H amination reaction (Figure 1c).

Results and Discussion

We recently demonstrated that the reaction of Ni^{II} complex **4** with *N*-fluoro-2,4,6-trimethylpyridinium triflate (NFTPT) results in rapid oxidation and intramolecular C(sp^2)–H activation to afford the Ni^{IV} σ-aryl product **5** (X = F) (Figure 2).[10] To achieve the catalytic cycle in Figure 1, this Ni^{IV} complex would need to undergo functionalization to afford **6**. As such, our initial studies explored the reactivity of **5** (with X = OTf to generate a better leaving group) with nucleophiles. However, the treatment of **5** with a variety of different nucleophiles (e.g., fluoride, chloride, acetate, phenoxide) under numerous different reaction conditions resulted in no trace of the corresponding functionalized organic product **6** (see Supporting Information for the reaction conditions examined). We hypothesize that this is due to the lack of an open coordination site *cis* to the σ-aryl ligand, which precludes inner-sphere C(sp^2)–Nuc bond-forming reductive elimination to generate **6**.[9d,11]

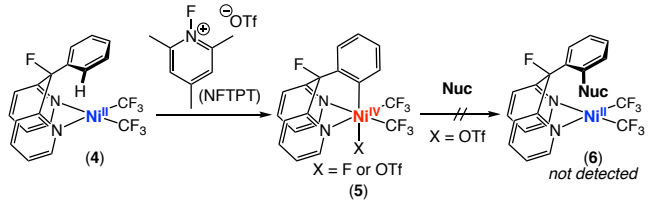

Figure 2. Previously reported C(sp^2)–H activation at Ni^{IV} and unsuccessful attempts to functionalize the Ni^{IV} σ-aryl product **5**

We noted that C(sp^3)–Nuc coupling reactions at Ni^{IV} are known to proceed via outer-sphere pathways that do not require *cis*-coordination of the nucleophile to the metal center.[9a-c,12] However, the cleavage of unactivated C(sp^3)–H bonds at high valent Ni centers is currently unprecedented.[13] To assess the feasibility of this transformation, we explored the oxidatively-induced C(sp^3)–H activation with Ni^{II} starting material **1**, which is an alkyl analogue of **4** (Figure 3). Complex **1** was synthesized via the reaction of ligand **7** with $(MeCN)_2Ni(CF_3)_2$. Ligand substitution proceeded within 20 min at room temperature in dichloromethane to afford **1** in 88% yield (Figure 3). The ^{19}F NMR spectrum of **1** shows the expected singlet for the CF_3 ligands (at –29 ppm) as well as a singlet for the fluorine on the bipyridine ligand (at –142 ppm). Notably, this latter signal shifts upfield by more than 25 ppm upon oxidation of the Ni center. As such, it serves as a convenient spectroscopic handle for monitoring the conversion of **1** to **2**. The X-ray structure of **1** shows two crystallographically independent molecules in the asymmetric unit. Both have square planar geometries, and the average distance between the Ni^{II} center and C1 is 2.940 Å.

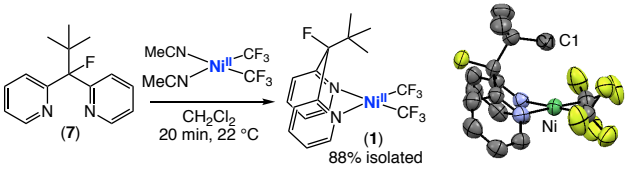

Figure 3. Synthesis of **1** and ORTEP diagram at 50% probability level (one of two molecules in unit cell is shown). Ni–C1 2.9313(4) and 2.948(4) Å (in two molecules in unit cell).

The reaction of **1** with NFTPT was conducted using conditions directly analogous to those for converting **4** → **5** (in dichloromethane at room temperature using 1.3 equiv of NFTPT; Figure 4). The reaction was monitored via ^{19}F NMR spectroscopy using the fluorine on the ligand as a spectroscopic handle. Within 10 min, complete consumption of the starting material was observed along with the appearance of two products (δ = –178 and –176 ppm) in a 4 : 1 ratio. These signals are consistent with the formation of two different diamagnetic Ni^{IV} products, which were ultimately assigned as **2-F[HPyMe$_3^+$]** and **2-OTf** (*vide infra*). A new singlet at –242 pm was also observed in the crude ^{19}F NMR spectrum. Both the chemical shift and integration of this signal suggest that the major product contains a Ni^{IV}–F bond.[10] The crude reaction mixture was also interrogated by ^1H NMR spectroscopy to confirm that C(sp^3)–H activation had occurred. The ^1H NMR spectrum shows singlets at 3.87 and 3.41 ppm in a 1 : 4 ratio, consistent with the formation of two Ni^{IV} σ-alkyl products.

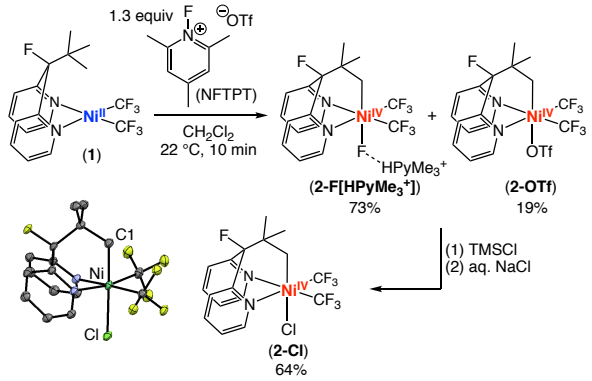

Figure 4. Oxidatively induced C-H activation and ORTEP diagram of **2-Cl** at the 50% probability level (solvent molecule omitted for clarity, one of two crystallograpically independent molecules in asymmetric unit is shown). Average Ni–C1 2.021 Å.

Treatment of this crude reaction mixture with 1.3 equiv of TMSCl followed by aqueous NaCl resulted in quantitative conversion to a single Ni^{IV} product, **2-Cl** (Figure 4). This complex was isolated in 65% yield and was characterized by ^1H, ^{19}F, and ^{13}C NMR spectroscopy as well as X-ray crystallography. The ^{19}F NMR spectrum shows a ligand resonance at –176.0 ppm, consistent with a diamagnetic Ni^{IV} complex. The ^1H NMR spectrum shows a singlet at 1.06 ppm that integrates to 6 protons, corresponding to the two equivalent methyl groups. The protons

of the Ni^{IV} σ-alkyl appear as a singlet at 3.71 ppm. The X-ray crystal structure of **2-Cl** (Figure 4) shows the expected octahedral geometry with an average Ni–C1 bond distance of 2.021 Å.

Complex **2-Cl** was then used as a starting material to establish the structure of the oxidation intermediates in Figure 4. The treatment of **2-Cl** with 5 equiv of AgF afforded **2-F** in 78% isolated yield (Figure 5). While the ^{19}F NMR signal for the ligand of **2-F** is identical to that of the major product formed *in situ* (δ = –178 ppm), the Ni^{IV}–F signal is shifted by more than 30 ppm to –274 ppm. This led us to hypothesize that the compound formed *in situ* is a collidinium adduct, in which the basic fluoride ligand reacts with the collidinium triflate formed during the C(sp^3)–H activation step. Consistent with this proposal, the treatment of **2-F** with 1 equiv of collidinium triflate ($HpyMe_3$OTf) quantitatively afforded **2-F[$HPyMe_3^+$]**, which is spectroscopically identical to the *in situ* product.

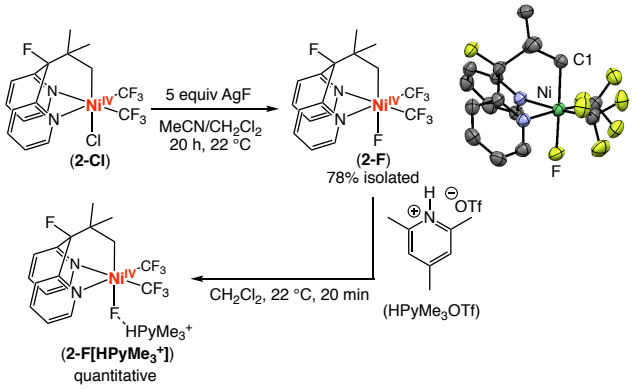

Figure 5. Conversion of **2-Cl** to **2-F** and **2-F[$HPyMe_3^+$]**. ORTEP diagram of **2-F** at the 50% probability level (one of two crystallograpically independent molecules in asymmetric unit is shown). Average Ni–C(sp^3) 1.999 Å, Ni–F 1.891 Å.

We hypothesized that the minor product formed *in situ* was the triflate complex **2-OTf**. This complex was independently synthesized via the treatment of **2-Cl** with TMSOTf (Figure 6). The ^{19}F and ^1H NMR spectra match those associated with the minor product observed in the oxidation reaction. The X-ray structure of **2-OTf** was obtained, and an ORTEP diagram is shown in Figure 6. Notably, the triflate is bound to Ni (Ni–O = 2.073 Å), despite being a relatively non-coordinating counterion. This is likely due to the high electrophilicity of the Ni^{IV} center.

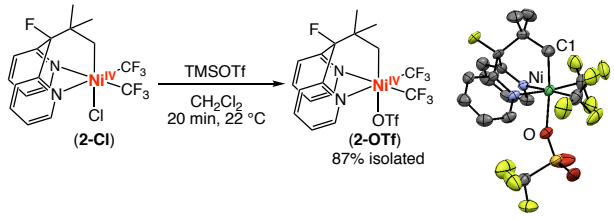

Figure 6. Synthesis of **2-OTf** from **2-Cl**. ORTEP diagram of **2-OTf** at the 50% probability level. Ni–C(sp^3) 2.000(3) Å, Ni–O 2.073(2) Å.

We next undertook DFT studies to interrogate the mechanism of this C(sp^3)–H activation reaction and to compare it to the previously studied C(sp^2)–H activation that forms complex **5** (Figure 2).[14,15] Two different pathways were examined: (1) a singlet reaction profile involving C(sp^3)–H activation at a Ni^{IV} intermediate and (2) a triplet pathway involving C(sp^3)–H cleavage occurring at a Ni^{III} center.

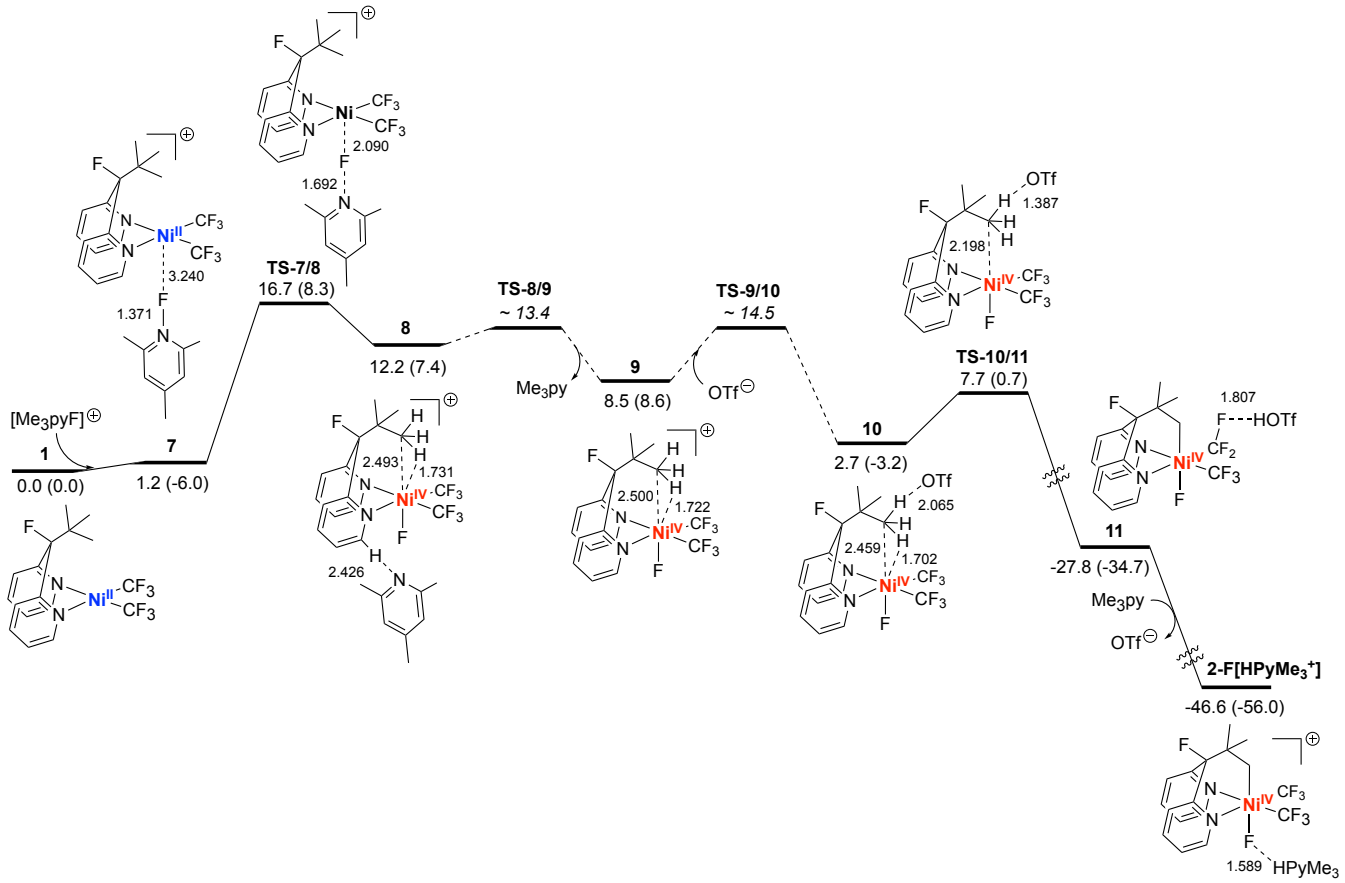

Figure 7. Singlet reaction pathway involving C(sp^3)–H activation at Ni^{IV} intermediate **12** via **TS_10/11**. Energies ΔG (ΔH) in kcal/mol relative to **1**.

The singlet profile is shown in Figure 7,[16] and it closely resembles that obtained for the C(sp^2)–H activation reaction (**4** → **5**).[10] The initial two-electron oxidation of **1** with NFTPT proceeds via **TS-7/8** with a barrier of 16.7 kcal/mol. This is nearly identical to that for the analogous oxidation of **4** (16.9 kcal/mol),[17,18] and it represents the highest energy step in the singlet reaction pathway. The Ni^{IV} product is adduct **8**, which undergoes dissociation of Me$_3$py followed by interaction with triflate to form **10**.[19,20] A low barrier triflate-assisted C(sp^3)–H activation then proceeds with a transition state energy of 7.7 kcal/mol (**TS-10/11**). Notably, a pathway involving triflate-assisted C(sp^3)–H activation at adduct **8** is considerably higher energy (+4.7 kcal/mol relative to **TS-9/10**; Figure S2).

Adduct **8** and structure **9** exhibit short interactions between Ni and the *t*-butyl group, with Ni···H distances of 1.731 and 1.722 Å. These interactions are likely a result of the high electrophilicity of this cationic Ni^{IV} center and the presence of an empty coordination site. Notably, in the analogous arene system, this electrophilicity is reflected in a very short Ni···C$_{ipso}$ interaction (Ni···C = 2.408 Å).[10] Interaction of triflate with **9** to form the proton transfer precursor **12** does not impact the Ni···^{t}Bu distance. Outer-sphere proton transfer proceeds from **10** with a low barrier (5.0 kcal/mol) to afford the Ni^{IV} σ-alkyl product.[21]

A second possible pathway for the conversion of **1** to **2** involves C(sp^3)–H cleavage at a Ni^{III} center (Figure 8).[16] A minimum energy crossing point (MECP) was identified that connects the singlet structure **8** (the initial intermediate in the singlet profile) with the triplet structure **12**. Triplet **12** exhibits spin density at Ni (1.10 e^-/Å^3), the fluoride ligand (0.29 e^-/Å^3), and the nitrogen of Me$_3$py (0.71 e/Å^3). As such, it can be formally assigned as [Me$_3$pyF]$^{\bullet+}$ and [Ni^{III}]$^{\bullet}$ fragments. In **12**, the Ni···^{t}Bu distance is ~0.6 Å longer than in Ni^{IV} species **8** and **9**, indicating minimal interaction in this system. This is consistent with the nature of the SOMO centered at Ni, which is a singly occupied d$_{z2}$-like orbital.

Interaction of **12** with triflate yields the adduct **15**. Attempts to locate a transition state for deprotonation from **15** failed, with potential energy scans leading to high energies during the relevant calculation. This is believed to be due to the half-filled d$_{z2}$-like orbital at Ni, which precludes acceptance of a pair of electrons upon proton transfer to triflate. However, C(sp^3)–H cleavage at Ni^{III} can occur via initial scission of the N–F bond (via **TS-13/14**) and subsequent electron transfer from triflate to [Me$_3$py]$^{\bullet+}$ to afford **15**. The triflate is now formally [OTf]$^{\bullet}$, and this doublet can abstract a hydrogen atom from the ^{t}Bu group via **TS-15/16** to afford triplet **16**. Finally, recombination between the alkyl radical and Ni^{III} affords the Ni^{IV} σ-alkyl product.[5] The highest energy step in this sequence is H• abstraction, which has a transition state (**TS-15/16**) at 17.3 kcal/mol. Notably, this is ~1 kcal/mol higher than the transition state for the oxidation step, and ~3 kcal/mol higher than any other transition state on the singlet pathway.

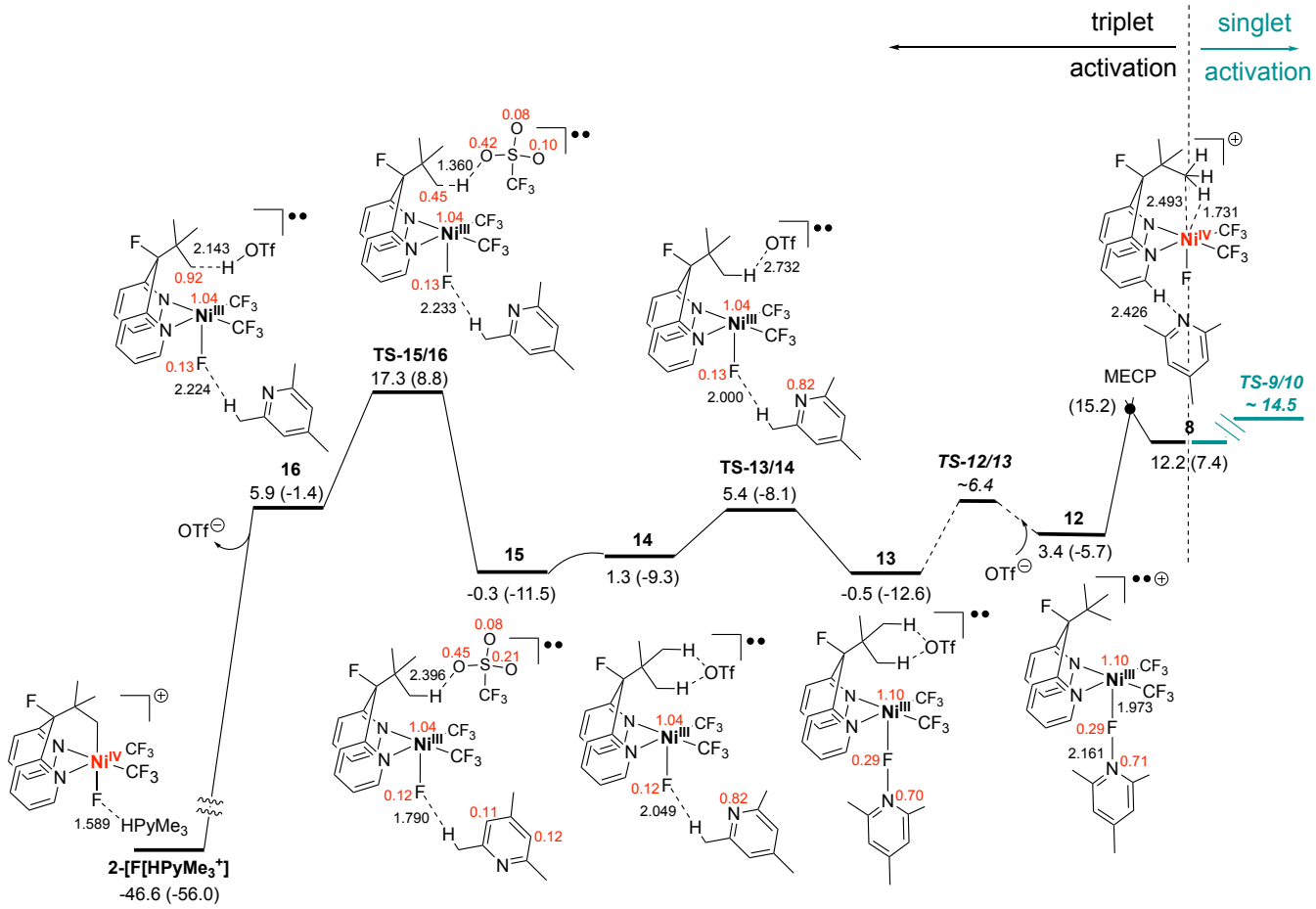

Figure 8. Triplet reaction pathway involving C(sp^3)–H activation at Ni^{III} intermediate **17** via **TS_15/16**. Energies ΔG (ΔH) in kcal/mol relative to **1**.

Overall, the DFT analysis presented here illustrates two possible pathways for the reaction of Ni^{II} reagent **1** with NFTPT to afford the Ni^{IV} C(sp^3)–H activation product. While the Ni^{IV} profile is ~3 kcal/mol lower in energy, this study suggests that both reaction manifolds could be accessible, particularly upon changing the substrate, supporting ligands, or reaction conditions. Overall, this DFT analysis further highlights the rich mechanistic pathways available in the organometallic and catalytic chemistry of nickel.

We next explored the reactivity of this Ni^{IV} σ-alkyl complex with nucleophiles to generate products of general structure **3**. Notably, this transformation would complete a formal catalytic cycle for the C(sp^3)–H functionalization of substrate **7**. Since fluoride is the strongest nucleophile associated with the oxidant NFTPT, we initially explored the reaction of **2** with F^-. As shown in Figure 9, the treatment of an *in situ* formed mixture of **2-F[HPyMe$_3$$^+$]** and **2-OTf** with 2 equiv of anhydrous tetramethylammonium fluoride (NMe_4F) at room temperature for 2 h resulted in C(sp^3)–F coupling to generate product **3-F** in 23% yield. Notably, this is the first reported example of C(sp^3)–F bond formation from a high valent Ni center.[22,23] The mass balance in this reaction is the Ni^{IV}–F complex **2-F**, which is formed via the deprotonation of **2-F[HPyMe$_3$$^+$]** by NMe_4F. When the analogous reaction was performed using **2-OTf** as the starting material, **3-F** was formed in higher yield (36%) along with significant quantities of **2-F** (34%). In contrast, when the reaction was conducted using **2-F**, less than 2% yield of the C(sp^3)–F coupled product was observed.[24] Overall, these results implicate **2-OTf** as the primary reactive species in this nucleophilic functionalization reaction, and suggest that there is a competition between fluoride attack at C_α (to form **3-F**) and at Ni^{IV} (to form **2-F**). The low relative reactivity of **2-F** is likely due to the poor leaving group ability of fluoride under the reaction conditions.

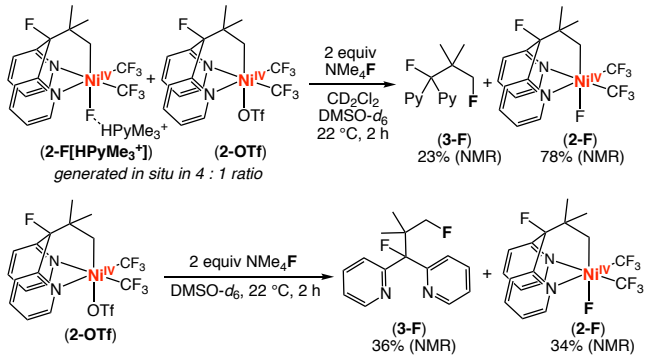

Figure 9. Ni–C(sp^3) fluorination with TMAF.

We next explored the scope of nucleophiles (X^-) that react with **2-OTf** to afford C(sp^3)–X coupled products (Figure 10). These reactions were monitored via ^{19}F NMR spectroscopy over 2 h at temperatures ranging from 22-60 ºC in either MeCN or DMSO. Heteroatom nucleophiles, including acetate, phenoxide, methyl malonate, phthalimide, and thiophenoxide, react with **2-OTf** to form products containing new C(sp^3)–O, C(sp^3)–N, or C(sp^3)–S bonds (**3**). The use of cyanide and lithium 2,4-pentanedionate as nucleophiles resulted in C(sp^3)–carbon bond

formation to afford **3-CN** or **3-dione**, respectively. Finally, with chloride as a nucleophile, product **3-py**$^+$ was formed, presumably via initial C–Cl coupling followed by intramolecular displacement of the chloride by a tethered pyridine. Notably, the reactions in Figure 10 were conducted under standard conditions for consistency. However, the rate of this functionalization reaction varies dramatically with the nucleophile, as would be expected for an S_N2-type mechanism. For instance, with fluoride as the nucleophile, the reaction is complete within 10 min, while with OAc the reaction takes the full 2 h under otherwise identical conditions.

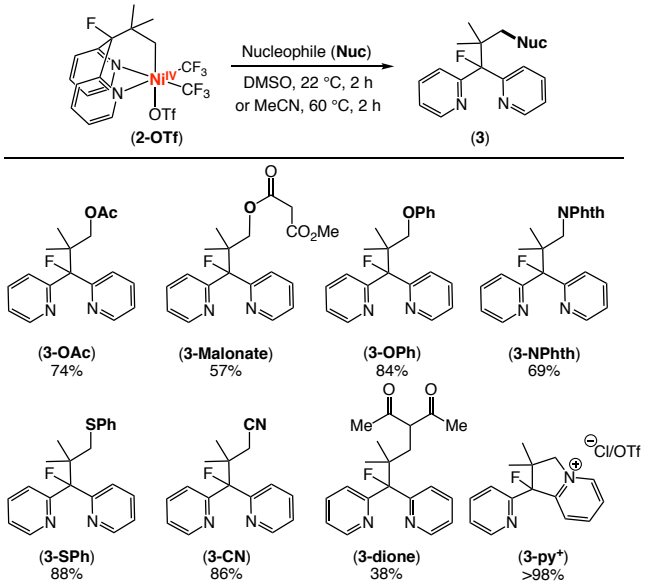

Figure 10. Functionalization reactions of **2-OTf**. Reported yields were determined via ^{1}H NMR spectroscopic analysis of the crude reaction mixture vs an internal standard. The identity of the functionalized products was confirmed by isolation and subsequent characterization via ^{1}H, ^{13}C, and ^{19}F NMR spectroscopy and HRMS. See SI for full experimental details on each reaction

The stoichiometric studies outlined above demonstrate the feasibility of two key steps of the Ni$^{II/IV}$-catalyzed C(sp^3)–H functionalization reaction outlined in Figure 11. Thus, our final investigations focused on establishing the viability of achieving catalytic turnover in this system. Importantly, the catalytic functionalization of highly engineered model substrates like **3** is not, in and of itself, of high interest in synthetic organic chemistry. Nonetheless, the ability to turnover this system under mild conditions would serve as the first proof-of-principle that high valent Ni-catalyzed C–H functionalization manifolds are feasible and could ultimately be translated to systems that are of broader synthetic utility. We anticipated several key challenges for translating the stoichiometric studies to catalysis. First, product **3** is expected to be a good ligand for Ni^{II}, which could lead to product inhibition and/or over-functionalization processes. As such, we sought to identify a system that limits product binding to the Ni center. Second, the stoichiometric studies suggest that functionalization of Ni^{IV}–F complex **2-F** is extremely slow relative to analogous reactions of **2-OTf**. Thus, we pursued strategies to minimize the formation of the former complex as an intermediate during catalysis. Finally, the oxidant NFTPT is susceptible to undesired side reactions with nucleophiles.[25,26] As such, we focused on identifying systems/conditions in which this competing side reaction is relatively slow.

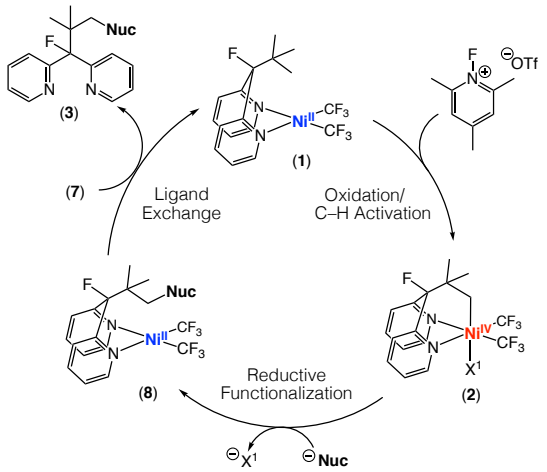

Figure 11. Putative catalytic cycle for the Ni$^{II/IV}$-catalyzed C(sp^3)–H functionalization of **7**

We reasoned that chloride would be an ideal choice of nucleophile for catalysis to address the first two challenges. As shown in Figure 10, the reaction of **2-OTf** with Cl$^-$ affords the pyridinium product **3-py**$^+$. This cyclized product should be a significantly weaker ligand than substrate **7**. Second, the chloride is expected to compete with fluoride as a ligand for the Ni^{IV} center, thus limiting catalyst sequestration as **2-F**.[27] We further hypothesized that catalyst sequestration could be further mitigated by slow addition of NFTPT to the reaction mixture. Finally, slow addition should also limit undesired side reactions between the oxidant and the chloride nucleophile.

After some optimization, we identified conditions that enable catalyst turnover in the C(sp^3)–H functionalization of **7** to form **3-py**$^+$ with **1** as the catalyst. The reaction proceeds best in a mixed solvent system of CH_2Cl_2 (the optimal solvent for the oxidation step) and DMSO (the optimal solvent for the functionalization). A 0.2 M solution of NFTPT in a 1:1 mixture of CD_2Cl_2:DMSO-d_6 was added via syringe pump at a rate of 0.2 mL/h. To limit undesired reactions between the oxidant and nucleophile, tetramethyl ammonium chloride (NMe_4Cl) was used as the limiting reagent. The substrate **7** was used in excess (3 equiv) to accelerate ligand substitution. Using 20 mol % of the Ni^{II} catalyst **1**, the product **3-py**$^+$ was formed in 76% yield after just 5 h at 40 ºC. While the TON remains modest (~4), this represents the first example of a catalytic C–H functionalization reaction involving C–H activation at high valent nickel. Furthermore, these are among the mildest conditions reported for a Ni-catalyzed C(sp^3)–H functionalization, highlighting the potential advantages of leveraging C–H cleavage pathways at high valent Ni centers.

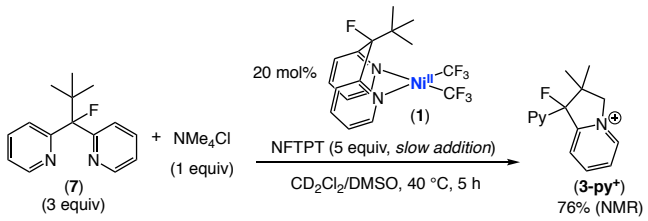

Figure 12. Catalytic C(sp^3)–H functionalization of **7**

In conclusion, this Article demonstrates that unactivated C(sp^3)–H bonds can be cleaved and subsequently functionalized at high valent Ni centers under mild conditions. Furthermore, these two steps can be coupled to achieve a proof-of-principle

catalytic transformation for the conversion of a C(sp^3)–H bond to a C(sp^3)–N bond. Currently, catalyst turnover in this transformation is limited by competing decomposition of the oxidant. As such, future work should focus on identifying next-generation catalyst/oxidant pairs for which the oxidation/C–H activation/functionalization sequence out-competes oxidant decomposition pathways. Overall, this study provides a template for the future development of catalytic transformations that exploit the unique reactivity of high valent Ni intermediates.

ASSOCIATED CONTENT

Experimental details, optimization tables, and complete characterization data for all new compounds. This material is available free of charge via the Internet at http://pubs.acs.org.

AUTHOR INFORMATION

Corresponding Author

mssanfor@umich.edu

Author Contributions

[#]These authors contributed equally.

Notes

The authors declare no competing financial interests.

ORCID

Melanie S. Sanford: 0000-0001-9342-9436
Allan J. Canty: 0000-0003-4091-6040
Alireza Ariafard: 0000-0003-2383-6380
Courtney C. Roberts: 0000-0001-8177-4013

ACKNOWLEDGMENT

This work was supported by the National Science Foundation Grant CHE-1111563 as well as CHE-0840456 for X-ray instrumentation. E.C. thanks NSERC for a postdoctoral fellowship. We gratefully acknowledge Emily Norwine for the characterization of product **3-OAc**.

REFERENCES

[1] (a) C-H Bond Activation and Catalytic Functionalization I; Dixneuf, P. H., Doucet, H., Eds.; Topics in Organometallic Chemistry; Springer International Publishing, 2016. (b) C-H Bond Activation and Catalytic Functionalization II; Dixneuf, P. H., Doucet, H., Eds.; Topics in Organometallic Chemistry; Springer International Publishing, 2016. (c) Yu; J.-Q. Shi, Z. C-H Activation, 1st ed.; Topics in Current Chemistry; Springer-Verlag Berlin Heidelberg: Heidelberg, 2010. (d) Gandeepan, P.; Muller, T.; Zell, D.; Cera, G.; Warratz, S.; Ackermann, L. 3d transition metals for C–H activation. *Chem. Rev.* **2019**, *119*, 2192-2452. (e) Rosen, B. M.; Quasdorf, K. W.; Wilson, D. A.; Zhang, N.; Resmerita, A.-M.; Garg, N. K.; Percec, V. Nickel-catalyzed cross-couplings involving carbon-oxygen bonds. *Chem. Rev.* **2011**, *111*, 1346-1416.

[2] Tasker, S. Z.; Standley, E. A.; Jamison, T. F. Recent advances in homogeneous nickel catalysis. *Nature*, **2014**, *509*, 299-309.

[3] Ananikov, V. P. Nickel: The "spirited horse" of transition metal catalysis. *ACS Catal.* **2015**, *5*, 1964-1971.

[4] Bour, J. R.; Ferguson, D. M.; McClain, E. J.; Kampf, J. W.; Sanford, M. S. Connecting organometallic Ni(III) and Ni(IV): Reactions of carbon-centered radicals with high-valent organonickel complexes, *J. Am. Chem. Soc.* **2019**, *141*, 8914-8920.

[5] (a) Beattie, D. D.; Grunwald, A. C.; Perse, T.; Schafer, L. L.; Love, J. A. Understanding Ni(II)-mediated C(sp^3)–H activation: Tertiary ureas as model substrates *J. Am. Chem. Soc.* **2018**, *140*, 12602-12610. (b) Omer, H. M.; Liu, P. Computational study of Ni-catalyzed C–H functionalization: Factors that control the competitive oxidative addition and radical pathways. *J. Am. Chem. Soc.* **2017**, *139*, 9909-9920.

[6] For reviews on Ni-catalyzed C–H functionalization with aminoquinolines and other directing groups, see: (a) Castro, L. C. M.; Chatani, N. Nickel catalysts/*N,N'*-bidentate directing groups: An excellent partnership in directed C–H activation reactions. *Chem. Lett.* **2015**, *44*, 410–421. (b) Yang, X.; Shan, G.; Wang, L.; Rao, Y. Recent advances in transition metal (Pd, Ni)-catalyzed C(sp^3)–H bond activation with bidentate directing groups. *Tetrahedron Lett.* **2016**, *57*, 819–836. (c) Potoschnig, G.; Maulide, N.; Schnürch, M. Direct functionalization of C–H bonds by iron, nickel, and cobalt catalysis. *Chem. Eur. J.* **2017**, *23*, 9206–9232. (d) Harry, N. A.; Saranya, S.; Ujwaldev, S. M.; Anilkumar, G. Recent advances and prospects in nickel-catalyzed C–H activation. *Catal. Sci. Technol*., **2019**, 9, 1726-1743. (e) Khake, S. M.; Chatani, N. Chelation-assisted nickel-catalyzed C−H functionalizations. *Trends in Chemistry* **2019**, *1*, 524-539.

[7] (a) Topczewski, J. J.; Sanford, M. S. Carbon–hydrogen (C–H) bond activation at Pd(IV): A frontier in C–H functionalization catalysis. *Chem. Sci.* **2014**, *6*, 70-76. (b) He, J.; Wasa, M.; Chan, K. S. L.; Shao, Q.; Yu, J.-Q. Palladium-catalyzed transformations of alkyl C–H bonds. *Chem. Rev.* **2017**, *117*, 8754-8786.

[8] For studies of C–H activation at high valent Pd, see: (a) Racowski, J. M.; Ball, N. D.; Sanford, M. S. C–H bond activation at palladium(IV) centers *J. Am. Chem. Soc.* **2011**, *133*, 18022-18025. (b) Maleckis, A. Kampf, J. W.; Sanford, M. S. A detailed study of acetate-assisted C–H activation at palladium(IV) centers. *J. Am. Chem. Soc.* **2013**, *135*, 6618-6625.

[9] (a) Roberts, C. C.; Camasso, N. M.; Bowes, E. G.; Sanford, M. S. Impact of oxidation state on reactivity and selectivity differences between nickel(III) and nickel(IV) alkyl complexes. *Angew. Chem. Int. Ed.* **2019**, *58,* 9104-9108. (b) Camasso, N. M.; Sanford, M. S. Design, synthesis, and carbon-heteroatom coupling reactions of organometallic nickel(IV) complexes. *Science* **2015**, *347*, 1218-1220. (c) Bour, J. R.; Camasso, N. M.; Meucci, E. A.; Kampf, J. W.; Canty, A. J.; Sanford, M. S. Carbon–carbon bond-forming reductive elimination from isolated nickel(III) complexes. *J. Am. Chem. Soc.* **2016**, *138*, 16105-16111. (d) Watson, M. B.; Rath, N. P.; Mirica, L. M. Oxidative C–C bond formation reactivity of organometallic Ni(II), Ni(III), and Ni(IV) complexes. *J. Am. Chem. Soc.* **2017**, *139*, 35-38. (e) Zheng, B.; Tang, F.; Luo, J.; Schultz, J. W.; Rath, N. P.; Mirica, L. M. Organometallic nickel(III) complexes relevant to cross-coupling and carbon–heteroatom bond formation reactions. *J. Am. Chem. Soc.* **2014**, *136*, 6499-6504. (f) Schultz, J. W.; Fuchigami. K.; Zheng, B.; Rath, N. P.; Mirica, L. M. Isolated organometallic nickel(III) and nickel(IV) complexes relevant to carbon-carbon bond formation reactions. *J. Am. Chem. Soc.* **2016**, *138*, 12928-12934. (g) D'Accriscio, F.; Borja, P.; Saffon-Merceron, N.; Fustier-Boutignon, M.; Mézailles, N.; Nebra, N. C–H bond trifluoromethylation of arenes enabled by a robust, high-valent Ni(IV) complex. *Angew. Chem., Int. Ed.* **2017**, *56*, 12898–12902.

[10] Chong, E.; Kampf, J. W.; Ariafard, A.; Canty, A. J.; Sanford, M. S. Oxidatively induced C–H activation at high valent nickel. *J. Am. Chem. Soc.* **2017**, *139*, 6058-6061.

[11] For Pd^{IV}: (a) Qu, F., Khusnutdinova, J. R.; Rath, N. P.; Mirica, L. M. Dioxygen activation by an Organometallic Pd(II) Precursor: Formation of a Pd(IV)–OH Complex and Its C–O Bond Formation Reactivity. *Chem. Commun.* **2014**, *50*, 3036-3039. (b) Racowski, J. M.; Dick, A. R.; Sanford, M. S. Detailed study of C–O and C–C bond-forming reductive elimination from Stable $C_2N_2O_2$–ligated palladium(IV) complexes. *J. Am. Chem. Soc.* **2009**, *131*, 10974-10983. For Pt^{IV}: (a) Zhao, S. B.; Wang, R. Y.; Nguyen, H.; Becker, J. J.; Gagne, M. R. Electrophilic fluorination of cationic Pt-aryl complexes. *Chem. Commun.* **2012**, *48*, 443-445. (b) Yahav-Levi, A.; Goldberg, K. I.; Vigalok, A.; Vedernikov, A. N. Competitive aryl–iodide vs aryl–aryl reductive elimination reactions in Pt(IV) complexes: Experimental and theoretical studies. *J. Am. Chem. Soc.* **2008**, *130*, 724-731.

[12] (a) Petrone, D. A.; Ye, J.; Lautens, M. Modern transition-metal-catalyzed carbon–halogen bond formation. *Chem. Rev.* **2016**, *116*, 8003-8104. (b) Bonney, K. J.; Schoenebeck, F. Experiment and computation: A combined approach to study the reactivity of palladium complexes in oxidation sttaes 0 to IV. *Chem. Soc. Rev.* **2014**, *43*, 6609-6638. (c) Sehnal, P.; Taylor, R. J. K.; Fairlamb. I. J. S. Emergence of palladium(IV) chemistry in synthesis and catalysis. *Chem. Rev.* **2010**, *110*, 824-889. (d) Canty, A. J. Organopalladium and platinum chemistry in oxidising milieu as model for organic synthesis involving the higher oxidation states of palladium. *Dalton Trans.* **2009**, *47*, 10409-10417.

[13] For C(sp^3)–H activation of the α-C–H bonds of acetonitrile at Ni^{III}, see: Zhou, W.; Zheng, S.; Schultz, J. W.; Rath, N. P.; Mirica L. M. Aromatic Cyanoalkylation through Double C–H Activation Mediated by Ni(III) *J. Am. Chem. Soc.* **2016**, *138*, 5777-5780.

[14] Frisch, M. J.; Trucks, G. W.; Schlegel, H. B. Scuseria, G. E.; Robb,M. A.; Cheeseman, J. R.; Scalmani, G.; Barone, V.; Mennucci, B.; Petersson, G. A.; Nakatsuji, H.; Caricato, M.; Li, X.; Hratchian, H. P.; Izmaylov, A. F.; Bloino, J.; Zheng, G.; Sonnenberg, J. L.; Hada, M.; Ehara, M.; Toyota, K.; Fukuda, R.; Hasegawa, J.; Ishida, M.; Nakajima, T.; Honda, Y.; Kitao, O.; Nakai, H.; Vreven, T.; Montgomery, Jr. J. A.; Peralta, J. E.; Ogliaro, F.; Bearpark, M.; Heyd, J. J.; Brothers, E.; Kudin, K. N.; Staroverov, V. N.; Kobayashi, R.; Normand, J.; Raghavachari, K.; Rendell, A.; Burant, J. C.; Iyengar, S. S.; Tomasi, J.; Cossi, M.; Rega, N.; Millam, J. M.; Klene, M.; Knox, J. E.; Cross, J. B.; Bakken, V.; Adamo, C.; Jaramillo, J.; Gomperts, R.; Stratmann, R. E.; Yazyev, O.; Austin, A. J.; Cammi, R.; Pomelli, C.; Ochterski,

J. W.; Martin, R. L.; Morokuma, K.; Zakrzewski, V. G.; Voth, G. A.; Salvador, P.; Dannenberg, J. J.; Dapprich, S.; Daniels, A. D.; Farkas, O.; Foresman, J. B.; Ortiz, J. V.; Cioslowski, J.; and Fox, D. J. *Gaussian 09*, revision A.02; Gaussian, Inc.;, Wallingford CT, 2009.
[15] Lee, C. T.; Yang, W. T.; Parr, R. G. Development of the Colle-Salvetti correlation-energy formula into a functional of the electron density. *Phys. Rev. B* **1988**, *37*, 785-789. (b) Miehlich, B.; Savin, A.; Stoll, H.; Preuss, H. Results obtained with the correlation energy density functionals of Becke and Lee, Yang and Parr. *Chem. Phys. Lett*. **1989**, *157*, 200-206. (c) Becke, A. D. Density-functional thermochemistry. III. The role of exact exchange. *J. Chem. Phys*. **1993**, *98*, 5648-5652.
[16] Additional weak H···F interactions in species containing Me_3py, except for **TS-15/16** and **16**, are omitted for clarity and are shown in Supporting Information.
[17] We also explored an SET process for this oxidation, in which initial single electron transfer from Ni^{II} to NFTPT is followed by fluorine atom transfer (ref. 17). However, this process was found to be uncompetitive with **1**, as the initially formed triplet adduct **[1---Me$_3$pyF]$^{\bullet\bullet+}$** (Figure S1), computes as 5.8 kcal/mol above the barrier for F^+ transfer (**TS-9/10**).
[18] Umemoto, T.; Fukami, S.; Tomizawa, G.; Harasawa, K.; Kawada, K.; Tomita, K. Power and structure-variable fluorinating agents. The *N*-fluoropyridinium salt system. *J. Am. Chem. Soc.* **1990**, *112*, 8563-8575.
[19] Stationary points **TS-10/11** and **TS-11/12** were estimated using the protocol of Hartwig and Hall, in which the barrier for dissociation of a ligand is estimated from the ΔH value for this process (see ref. 19).
[20] (a) Hartwig, J. F.; Cook, K. S.; Hapke, M.; Incarvito, C. D.; Fan, Y.; Webster, C. E.; Hall, M. B. Rhodium boryl complexes in the catalytic, terminal functionalization of alkanes. *J. Am. Chem. Soc.* **2005**, *127*, 2538-2552. (b) Wei, C. S.; Jiménez-Hoyos, C. A.; Videa, M. F.; Hartwig, J. F.; Hall, M. B. Origins of the selectivity for borylation of primary over secondary C–H bonds satalyzed by Cp*-rhodium complexes. *J. Am. Chem. Soc*. **2010**, *132*, 3078-3091.
[21] The Me_3py can also act as the base for deprotonation, but with a higher barrier than that with triflate (+ 1.7 kcal/mol; Figure S3). We also note that triflate is at significantly higher concentration than Me_3py throughout the reaction, as the released Me_3py is rapidly protonated by HOTf.
[22] (a) Lee, H.; Börgel, J.; Ritter, T. Carbon–fluorine reductive elimination from nickel(III) complexes. *Angew. Chem. Int. Ed.* **2017**, *56*, 6966–6969. (b) Meucci, E. A.; Ariafard, A.; Canty, A. J.; Kampf, J. W.; Sanford, M. S. Aryl–fluoride bond-forming reactions at nickel(IV) centers. *J. Am. Chem. Soc.* **2019**, *141*, 13261-13267.
[23] Perez-Temprano, M. H.; Racowski, J. M.; Kampf, J. W.; Sanford, M. S. Competition between sp^3-C–N and sp^3-C–F reductive elimination from palladium(IV) Complexes. *J. Am. Chem. Soc.* **2014**, *136*, 4097-4100.
[24] The reaction of **2-Cl** with NMe_4F afforded **3-F** (44%) and **2-F** (37%).
[25] Umemoto, T.; Tomizawa, G.; Hachisuka, H.; Kitano, M. Novel base-initiated reactions of *N*-substituted pyridinium salts. *J. Fluor. Chem.* **1996**, *77*, 161–168.
[26] A variety of other oxidants were explored in this catalytic transformation, with a particular focus on other F^+ reagents such as NFSI and Selectfluor. In all cases, a maximum of a single catalyst turnover (10% yield) was obtained. This appears to be largely due to the necessity of the triflate counterion as well as the oxidant's ability to oxidize Ni that is not ligated.
[27] A variety of other nucleophiles were explored in this catalytic transformation, including cyanide, acetate, and lithium 2,4-pentandionate. In all cases, a maximum of a single catalyst turnover (10% yield) was obtained. This is largely due to binding of the nucleophile to the complex, which appears to inhibit catalysis.

Table of Contents Figure: